Journal of
Ceramic Science
and Technology

*J. Ceram. Sci. Technol.*, **12** [2] 71-80 (2021)
DOI: 10.4416/JCST2020-00020
available online at: http://www.ceramic-science.com


# 3D Printing of Zirconia Ceramic Slurry: Effect of Overlapping Rate on Surface Finish and Mechanical Properties

**J. Zhang[1], J. Zhou[2], J. Cai[1], G. Duan[*1]**

[1]School of Mechanical Engineering, Hebei University of Technology, Tianjin 300401, China
[2]School of Mechanical Engineering, Tianjin University of Science and Technology, Tianjin 300222, China
received August 9, 2020; received in revised form November 14, 2020; accepted May 24, 2021

**Abstract**

**This paper reports on how water-based zirconia ceramic for dentures has been successfully prepared for 3D printing based on a material extrusion process. The rheological properties of the ceramic slurry determine the process parameters, that is the buildability and formed quality of the printed samples. The rheological properties of the zirconia ceramic slurry have been explored to identify suitable process parameters. "Collapse" and "overlapping" models for the ceramic slurry filament have been developed to underpin the theoretical groundwork for selection of suitable printing parameters. Nozzles with inner diameters measuring 0.4 mm, 0.5 mm, 0.6 mm and 0.7 mm were selected for extrusion tests. The test results showed that, in spite of different nozzle diameters, all the height errors are below 5 %, indicating the rationality for the currently proposed "collapse" model. The surface finish and porosity of the printed samples before and after sintering were observed with a digital microscope. Surface roughness, density and mechanical properties of the printing samples were tested and measured. The experimental results show that for the nozzle inner diameter of 0.5 mm, when the overlapping rate of the filaments is set to 6.4 %, in accordance with the currently proposed "overlapping" model, the relative density of the printing sample is 0.99; while after sintering, a very desirable roughness of 1.4 µm and bending strength of 611.64 MPa are achieved. The rationality of the currently proposed "collapse" and "overlapping" models is comprehensively verified by the superior surface quality and mechanical properties of the printed samples. Setting of a suitable overlap rate is helpful for improving the printed quality of ceramic parts. The paper sheds light on precision improvement for 3D printing material extrusion technology in general.**

*Keywords: Zirconia ceramics, 3D printing material extrusion, filament collapse, overlap rate*

## I. Introduction

3D printing, alias additive manufacturing (AM), is an innovative and high-added-value technology for fabricating 3D structures with complex geometry by depositing materials layer by layer. Compared to other printing processes, such as vat photopolymerization, binder jetting, material jetting, powder bed fusion [1], the material extrusion process has been acclaimed as being the most cost-effective 3D printing process owing to its eco-friendliness, the single structure of the printer, and the easy plug-and-play access. On another positive note, a wide diversity of printable materials, such as polymers, metals, composites, biocompatible hydrogels, concrete, and ceramics in filament form, is available for the extrusion process. For different materials, respective commensurate printing parameters, such as extrusion pressure, scanning speed, and layer height, etc. [2–7], should be specified appropriately in order to yield reliable and robust printed parts. To this end, researchers have made significant efforts to optimize the extrusion process [8–9]. Although remarkable progress has been witnessed in the past few years, there is still room for improvement with regard to the printing quality.

* Corresponding author: glduan@hebut.edu.cn

In the extrusion-based 3D printing process, materials in filament form are the basic feedstocks. In a standard slurry-extrusion-based 3D printing process, the printing material is directly squeezed and pressed onto the build platform. Owing to gravity, the deposited materials in their green state inevitably deform. The deformation is escalated by the printing pressure to effect bonding between different layers. This undesirable deformation results in pores caused by the uneven line width, impairing the printing quality [10]. To evaluate the printing quality, two criteria have been proposed. One is fluidity to ensure smooth passage of the material through the nozzle for deposition; and the other is printability, enabling sufficient green strength to maintain stability of the printed structure immediately after deposition [11–14]. Only materials that meet both criteria can be extruded with fidelity, so as not to collapse during printing and post-processing (that is sintering) [15]. However, the dilemma is that if fluidity is too high, this will impede buildability. For an acceptable trade-off that balances fluidity and buildability, researchers have proposed an increase in the solid content of the slurry [16–17].

A significant feature of the material extrusion process is the ridged surface of the printed samples [18], which is a primary indicator of printing quality. The inherent ridged

surface is caused by two sources: one is the round shape of the extrusion nozzle [19], and the other is the overlap between extruded filaments. In the extrusion printing process, there are generally three positional co-relationships between adjacent filaments, as shown in Fig. 1. When the overlap rate is less than or equal to 0, as shown in Fig. 1(a) and Fig. 1(b), the filaments are in line contact or separated from each other, leaving gaps, which are registered as internal structural defects. When the overlap rate is greater than 0, overlap occurs between adjacent filaments, as shown in Fig. 1(c). If the overlap rate is too small and the gaps between the filaments are not filled sufficiently, the ridge effect results. It will effectuate internal structural gaps. This defect is contagious to all the following upper layers, so as to yield a wavey texture of the sample's exterior surface. On the other hand, if the overlap rate is too large, the ridge effect will be alleviated, but the shape of the filament will be distorted, leading to "over-deposition". With accumulation of "over-deposition" over the height, movement of the nozzle will be impeded, and the outlet of the nozzle will be blocked by the resultant ridge, impairing printing quality. Therefore, the overlap rate is the key parameter for the surface quality (printing quality), and thus the mechanical properties of the printed sample [20].

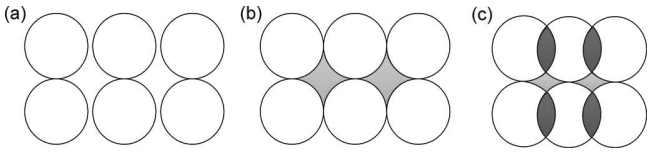


**Fig. 1:** Relative position between adjacent filaments: (a) separation, (b) line contact, (c) intersection.

The surface quality is indicated quantitatively by the three-dimensional shape, dimensional accuracy and roughness. Ji *et al.* established the relationship between printing parameters and roughness, and experiments showed that the deposition parameters had an impact on the surface morphology and roughness [21]. Comminal *et al.* numerically simulated the successive deposition of parallel beams to predict the porosity of interlayer bonding surfaces [22]. Luo *et al.* studied the characteristic size distribution of a single line by conducting line assembly experiments and derived that a satisfactory formed surface could be obtained by setting a suitable scanning distance [23]. However, no further discussion and verification of the quality of multi-layer shaping was provided. The mechanical performance of printed parts is an indication of their internal structural defects. Poorer performance indicates more internal structural defects. Serdeczny *et al.* analyzed the relationship between the offset distance and inter- and intra-layer bond line densities by numerically simulating the process of material extrusion to derive detailed distributions of porosity and roughness [24]. Eiliat *et al.* developed a C++ program to calculate the optimal line width and overlap rate to reduce the gap between each layer and avoid manufacturing internal chimneys [25]. Wang *et al.* reduced the step effect and improved the internal filling structure by studying the changing law of adaptive filament width [26].

In this study, the ceramic slurry is non-Newtonian, exhibiting obvious sedimentary deformation. It is understood that if the deformation of slurry is ignored, setting of the overlap rate will not be suitable, which has a severe impact on the printing quality of the ceramic slurry. Therefore, before calculation of the overlap rate, the cross-sectional size of the filament is derived by predicting the collapse and deformation of the filament. This research intends to produce ceramic samples with uniform morphology and excellent mechanical properties based on the setting of suitable overlap rate parameters. The rheological properties of zirconia ceramic slurry are studied. The "collapse" and "overlap" models of extruded filaments are established. Based on the optimization of the overlap rate parameters, ceramic samples with excellent surface quality and mechanical properties are produced.

## II. Material and Methods

### *(1) Slurry preparation*

The slurry is a mixture of four materials: sodium polyacrylate (PAAS) as a dispersant (50 % in water, Mw = 5100, Aladdin Biochemical Technology Co., Ltd., Shanghai, China), HIN-epoxy resin as a binder (MHR-070, Hubei Xitai Chemical Co., Ltd., China) and distilled water as a solvent were mixed in defined proportions. The pH value of the solution was adjusted to 10.8 with the addition of sodium hydroxide (Shanghai Aladdin Biochemical Technology Co., Ltd, China) at a concentration of 5 mol/L. The pH value was measured with a pH meter (PH510, Alalis Instruments Technology Co., Ltd, China), and the prepared solution was then placed into a 40 KHz ultrasonic cleaner and shaken for 3 min until a homogeneous mixture was obtained. Zirconia powder, consisting of 94.5 wt% yttrium (III)-oxide and 5.5 wt% zirconia with an average particle size of 300 nm, was used as the main raw material (3Y-TZP, Guangdong Oriental Zirconia Ind Sci & Tech Co., Ltd, China). The prepared solution was placed into a planetary ball mill (TJQ, Techin, Tianjin, China) and the mixture was then wet-milled for 5 h at 130 rpm with a ball-powder ratio of 4:1 until the mixture was converted into slurry. The flowchart for the 3D printing material extrusion process is sketched in Fig. 2.

### *(2) 3D printing device and extrusion steps*

The device used, as shown in Fig. 3, is our own in-house development of a pneumatic ceramic 3D printer based on micro-flow extrusion. The printable size of the 3D printer is 400 mm × 400 mm × 300 mm, the positioning accuracy is 0.02 mm, and the available nozzle inner diameter is 0.3 mm – 1.45 mm.

The device deposits layers continuously in a computer-controlled environment to create three-dimensional objects. The air pump provides the air pressure and pushes the piston to squeeze the ceramic slurry into the round tube of the nozzle. The pressure is controlled by the precision pressure-regulating valve to ensure smooth extrusion

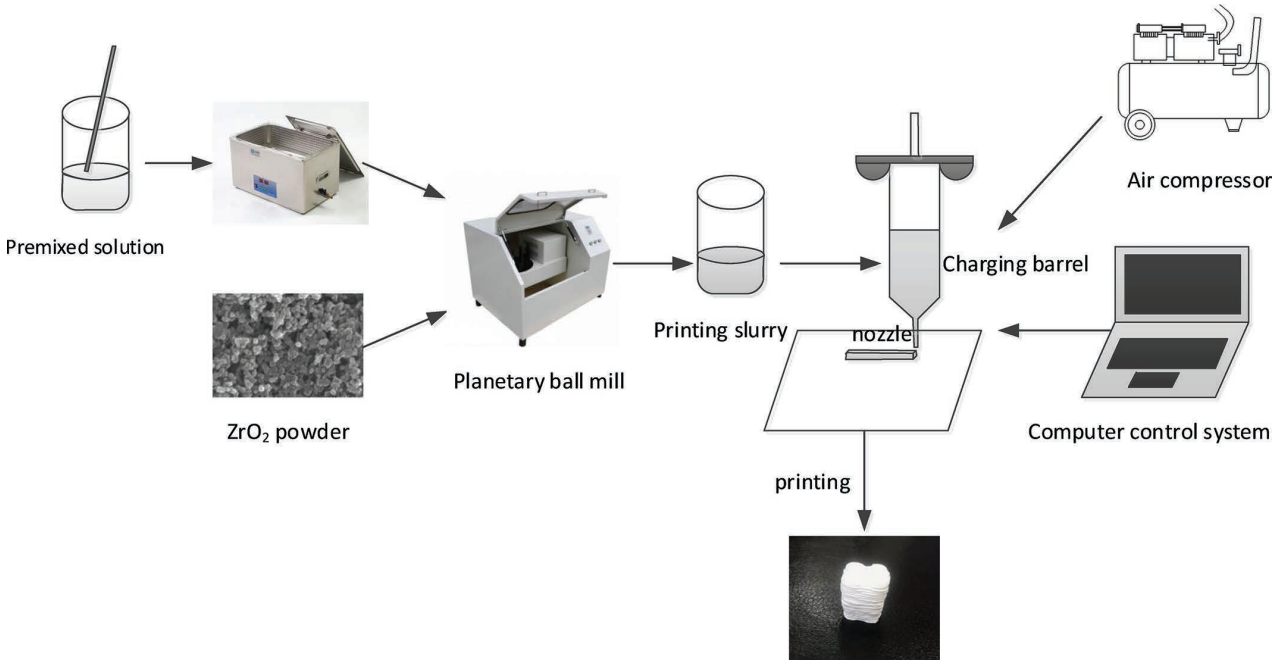


**Fig. 2:** Flowchart for 3D printing material extrusion process.

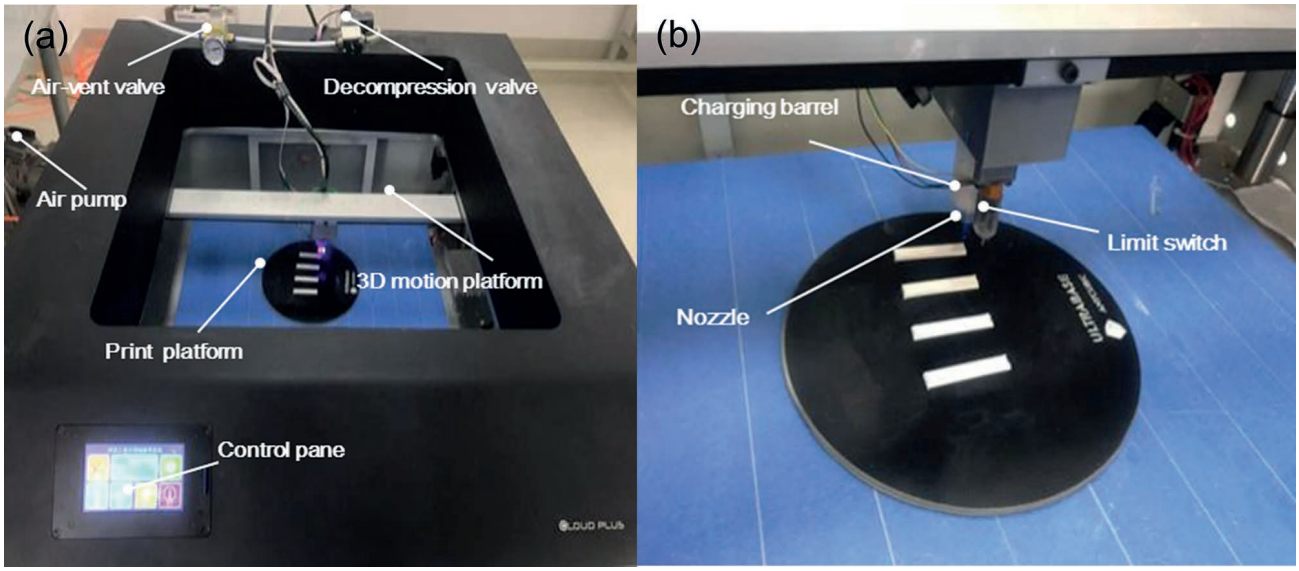


**Fig. 3:** Ceramic 3D printing machine: (a) overall view of ceramic 3D printer, (b) zoomed-in view of nozzle.

of the ceramic slurry. The three-dimensional motion platform realizes the spatial motion of the nozzle. The specific procedure for the process is as follows: After the nozzle completes the scanning of a single layer in the XY plane, the printing platform moves down a layer height along the Z axis. The ceramic slurry is accumulated layer by layer until the layers finally stack up to form the overall geometry of the printed sample. The relevant 3D printing parameters with different nozzle diameters in this study are listed in Table 1. Nozzles with diameters of 0.4 mm, 0.5 mm, 0.6 mm and 0.7 mm are used for the multi-layer sample extrusion according to the cross-sectional height of the filament obtained with the collapse model. The single-layer and multi-layer sample extrusion tests are carried out for a nozzle with a diameter of 0.5 mm in accordance with the optimum overlap rate obtained based on the overlap model. The single-layer sample has a size of 67 mm × 8 mm, and a sample with similar cross-sectional size and six identical layers is also built.

**Table 1:** Printing parameters for different nozzle diameters

| Nozzle (mm) | Printing speed (mm/s) | Extrusion pressure (MPa) | Layer height (mm) |
|---|---|---|---|
| 0.4 | 14 | 0.3 | 0.38 |
| 0.5 | 14 | 0.16 | 0.48 |
| 0.6 | 14 | 0.1 | 0.58 |
| 0.7 | 14 | 0.08 | 0.67 |

### *(3) Analytical models*

The ceramic slurry used in this study is viscoelastic fluid subject to pressure loading during the printing process, self-gravity as well as gravity from subsequent upper layers. Owing to self-gravity and pressure, the extruded filament bulges laterally to inevitably exhibit a collapse phenomenon. Since the upper and lower surfaces of the interlaminar filaments are approximately flat after adhesion, the cross-section of the filament approaches a drum shape, as shown in Fig. 4. For convenience of following derivation, relevant quantities are indicated in Fig. 4.

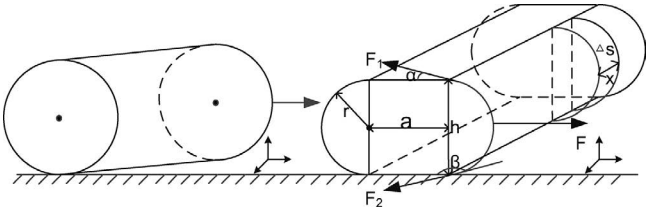


**Fig. 4:** Schematic for filament collapse.

A schematic showing the overlap is shown in Fig. 5. The overlap rate is defined as: $\text{overlap rate}(\%) = \frac{w}{W} \cdot 100\,\%$, where w is the overlap width of the filament and W is the total width of the two adjacent filaments, with provision for the overlap.

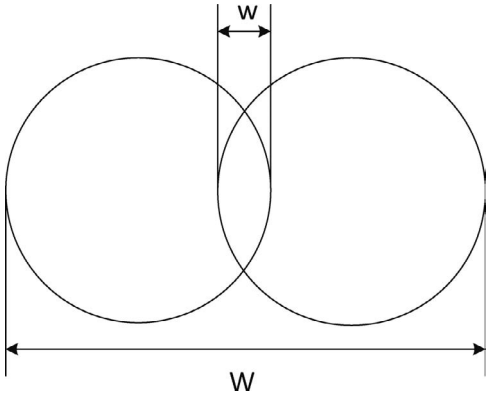


**Fig. 5:** Schematic for filament overlapping.

In surface layers, some surfaces of the filament are exposed to air. Owing to surface tension, the surfaces exposed to air tend to shrink. Therefore, the horizontal resultant force, of the upper and lower surface tension $F_1$ and $F_2$, is opposite to the lateral pressure of the slurry due to gravity $F$, as indicated in Fig. 4. On the side surface, the area element $\Delta S$ with width $x$ and height $h$ is selected. The angle between the upper surface tension and the horizontal direction is $\alpha$, and $\alpha \in (0, \frac{\pi}{2})$.The bottom surface of the filament is in contact with the solid owing to gravity, for convenience of calculation, the contact angle $\beta$ of the bottom surface of the filament is assumed to be 180°. Since the cross-section of the extruded filament is symmetrical, force analysis is only performed for the right side.

The resulting surface tension towards the medial side is

$$F_1 \cdot \cos\alpha + F_2 \cdot \cos(\pi - \beta) = \sigma \cdot x \cdot \cos\alpha + \sigma \cdot x \qquad (1)$$

$$F = f \cdot \Delta S \qquad (2)$$

where $\sigma$ denotes the coefficient of surface tension; $x$ represents the length of tension; $F$ symbolizes the lateral pressure of the slurry on $\Delta S$ owing to gravity.

The stress-strain relationship inside the filament can be linearly approximated as

$$f = K \cdot \gamma \qquad (3)$$

where $f$ is the stress in the filament; $\gamma$ is the strain along the horizontal direction of the strand cross-section; $K$ is a material variable in terms of the storage modulus of the material and strain $\gamma$ ($k=k(\gamma)$). It is understood that the smooth deposition of slurry depends on the rheological properties of the ceramic slurry, which can be reflected by K. The collapse deformation of the filament is exhibited only in the radial direction, so the cross-sectional area does not change, that is

$$\pi \cdot R^2 = \pi \cdot r^2 + a \cdot 2r \qquad (4)$$

When the cross-sectional shape of the deposited filament is considered to be stable, so that the force is in balance. In the horizontal direction, there is

$$\sigma \cdot x \cdot \cos\alpha + \sigma \cdot x = K \cdot \gamma \cdot (x \cdot h) \qquad (5)$$

where,

$$\gamma = \frac{a + 2r - 2R}{2R} \qquad (6)$$

To reduce the step effect and internal defects of the sample, the overlap cross-sectional area of the filament should be equal to the interstitial cross-sectional area of the filament, as shown in Fig. 6.

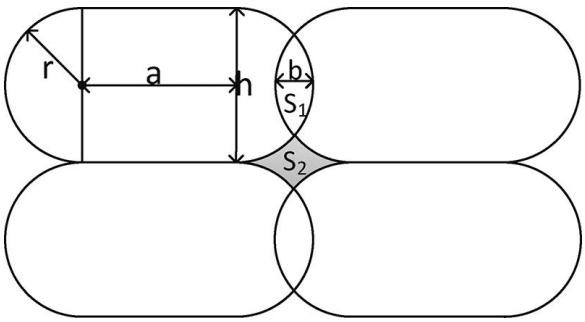


**Fig. 6:** Schematic for overlapping after slurry stand collapse.

That is

$$S_1 = S_2 \qquad (7)$$

The overlap area of adjacent filaments is

$$S_1 = 4 \int_{r-\frac{b}{2}}^{r} \sqrt{r^2 - x^2}\, dx \qquad (8)$$

The void area formed by adjacent filaments is

$$S_2 = r \cdot (2r - b) - \frac{1}{2}\pi \cdot r^2 + 2 \int_{r-\frac{b}{2}}^{r} \sqrt{r^2 - x^2}\, dx \qquad (9)$$

where $x$ is the horizontal distance of any point in the cross-section of overlap relative to the center of the circle. Therefore, the overlap rate is given as below,

$$\eta = \frac{b}{2r + a - b} \cdot 100\% \qquad (10)$$

### *(4) Physical characteristics*

A rotational rheometer (MCR 302, Anton Paar, Graz, A) is used to test the relationship between the storage modulus and strain of the zirconia ceramic slurry. The rheometer is equipped with a 50-mm diameter plate–plate geom-

etry, with a set temperature of 20 °C and a gap of 1 mm. The prepared zirconia ceramic slurry is sheared at a steadily increasing rate from 0.01 to 100 1/s with a frequency of 1 Hz. A contact angle measuring instrument (SZ-CAMC33, Sunzern, China) is used to measure the surface tension of the slurry. A three-dimensional surface profile meter (NanoMap-1000WLI, Aep technology, USA) with white light interference is adopted to measure the surface profile and roughness of the sample. A digital microscope (Smart Zoom 5, Zeiss, Germany) is employed to observe the morphological characteristics of the sample. The relative density of the specimen is measured with the Archimedes method. An electronic universal material testing machine (3365, Instron, USA) is used to conduct three-point bending tests on the sample with the size 63 mm × 6.5 mm × 2.3 mm at a displacement loading rate of 0.5 mm/min. A scanning electron microscope (Phenom ProX, Netherlands) is used for observing and analyzing the microscopic fracture characteristics of the samples. A digital vernier caliper (DL91150, Deli, China) is applied to measure the dimensions of the sample before and after sintering to calculate the shrinkage in each direction.

## III. Results and Discussions

Fig. 7 shows the measured storage modulus-strain relationship of the zirconia ceramic slurry. The curve-fitting relationship is given in Fig. 7. If the fitting result is substituted into formula (5), then, when the inner diameter of the nozzle is 0.4 mm, 0.5 mm, 0.6 mm and 0.7 mm, respectively, the corresponding cross-sectional heights of the extruded filaments after collapse are 0.38 mm, 0.48 mm, 0.58 mm and 0.67 mm. It can be inferred that all the rates of the collapsed cross-sectional heights of the extruded filament to the respective inner diameter of the nozzle approximate 0.96.

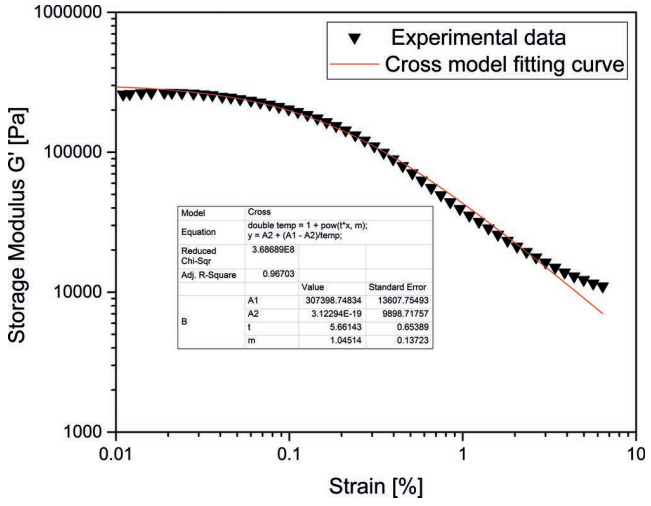


**Fig. 7:** Storage modulus-strain relationship of zirconia ceramic slurry.

### *(1) Dimensional precision*

The theoretical layer height from the current collapse model is used as the layer height during printing. In Fig. 8, the actual average layer height measured from the experiment is compared with the average layer height theoretically derived based on the currently proposed collapse model. The lines of the front view of the sample printed with nozzles of different inner diameters are uniform and clear, and the error between the actual and theoretical layer height is within 5 % as shown in Fig. 8, which shows that the collapse model is correct and effective and can be used as a guide for setting of a suitable overlap rate.

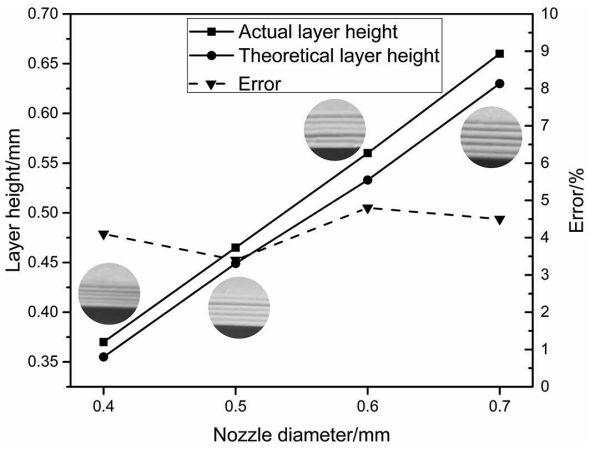


**Fig. 8:** Relation between nozzle diameter and layer height.

So, the different overlap rates have almost the same influence on shrinkage in the direction of length and height. In the direction of width, different overlap rates cause filament accumulation or voids in deposition, then the shrinkage rate is the largest and the change is the most obvious. When the overlap rate is 6.4 %, the overall shrinkage rate is the lowest in all directions.

In spite of different overlapping rates, the overall sizes of the ceramic samples printed with nozzle inner diameter of 0.5 mm shrink significantly after sintering, as shown in Fig. 9. From experiments, it is observed that the filament in the direction of length is extruded continuously without fracture, thus the inner texture of the filament is uniform and dense without pores. Owing to gravity, the newly deposited filament will cling to the previous layer vertically to exhibit directionally high bonding strength. Therefore, the influence of different overlap rates on shrinkage in the printing direction and height is similar. However, in the

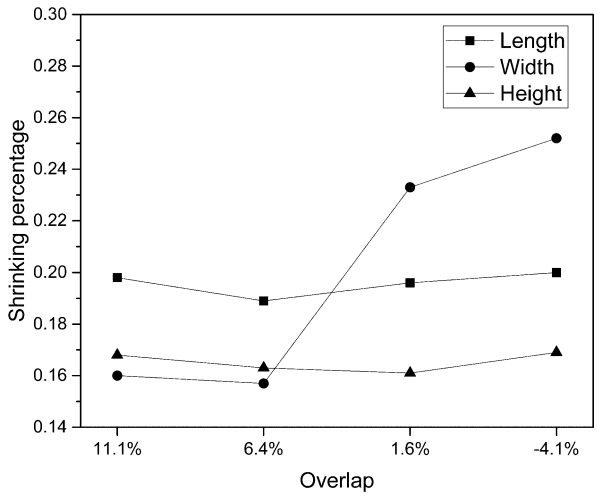


**Fig. 9:** Shrinkage variation of samples with different overlap rates in all directions.

direction perpendicular to the printing path, different overlap rates can cause neighboring filaments to overlap or disengage, so that the shrinkage rates are different after sintering. When the overlap rate is 6.4 %, the overall shrinkage rates of the sample in all directions are lowest.

### *(2) Morphological characteristics*

Theoretical calculation indicates that when the nozzle diameter is equal to 0.5 mm, the printing quality with overlap rate of 6.4 % is optimum. Fig. 10 shows the printed single-layer and multi-layer samples with different overlap rates before sintering. When the overlap rate is 11.1 %, slurry is excessively extruded to yield overlapping of adjacent filaments, resulting in increasing width of sample, no obvious surface texture, and relatively high layer height. As subsequent layers accumulate, the nozzle printing height is lower than the height of filament section, distorting the original morphology of the filament. Irregular texture on the surface of multi-layer samples and even scratches caused by the printhead are visible, as shown in Fig. 10(a). When the overlapping rate is 6.4 %, the surface texture of monolayer and multilayer samples is regular and clear. The filament deposits are dense and uniform, and the valleys are lowest, as shown in Fig. 10(b). This is because a suitable volume overlap can fill the ridges between adjacent filaments of the deposition layer, the filaments between adjacent layers collapse and deform under the action of gravity. In this way, not only the surface step effect can be reduced, but also the void of the internal structure can be reduced. After filament deposition, diffusion can make the bond between adjacent filaments closer and increase the adhesion, so the surface quality is optimal. When the overlapping rate is 1.6 % and -4.1 %, the single-layer sample has an obviously rough texture. There are even gaps between the strands, and observable defects, such as different strand diameters or pits are exhibited on the surface of the multi-layer sample, as shown in Fig. 10 (c-d). This is because overlap rates that are too low cause the filaments to stretch or collapse during the deposition process. The deposition process is therefore not stable.

The surface of a multi-layer sample after sintering is shown in Fig. 11 (a1-d1). Owing to the large shrinkage of the sample after high-temperature sintering, the surface texture is no longer regular as shown in Fig. 11 (a1). It is seen that Positions 1 and 2 are defects caused by the nozzle. The surface texture is regular and has no defects in Fig. 11 (b1). In Fig. 11 (c1), cracks appear between surface textures owing to shrinkage during sintering. These are attributed to the low bonding strength between the filaments. In Fig. 11 (d1), the filament diameter at Position 1 is relatively small, and a ridged surface is exhibited. As shown in Fig. 11 (a2-d2), the surface contours of multi-layer samples with different overlap rates can be observed. Meanwhile, with the increase of overlap rate, the surface roughness of the sample gradually increases, as shown in Fig. 11 (a3-d3).

The printing path follows a "zigzag" pattern so a "U"-shape connection appears at the turn of filaments in the side view of the sample. As shown in Fig. 12(a), the "U"-shape is closely arranged, and the "U"-shape between layers is severely distorted with protrusions or depressions, indicating that, owing to the small offset distance, the filaments appear to have been "over-deposited". Thus, the intended morphology is not achieved. In Fig. 12(b),

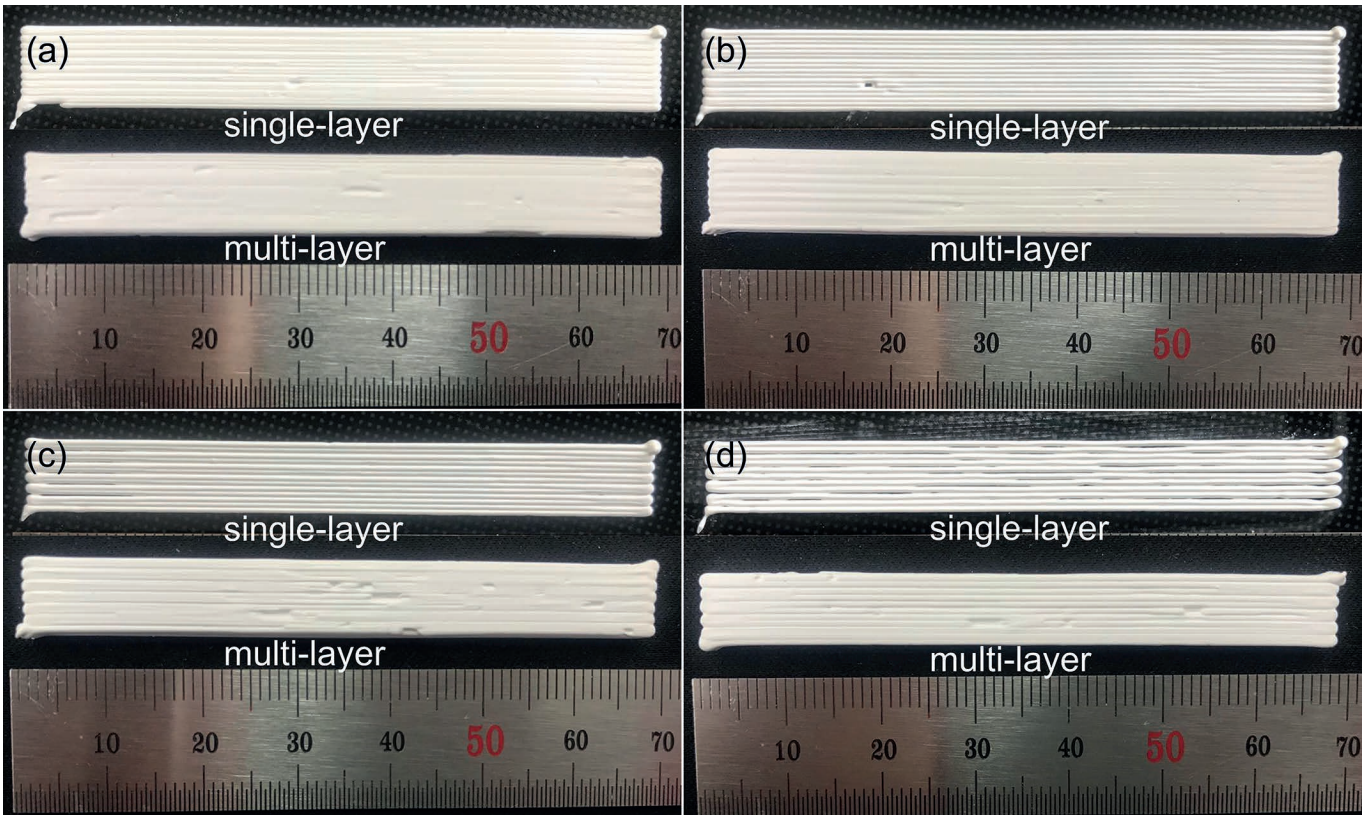


**Fig. 10:** Single-layer and multi-layer printed samples before sintering at different overlap rates: (a) 11.1 %, (b) 6.4 %, (c) 1.6 %, (d) -4.1 %.

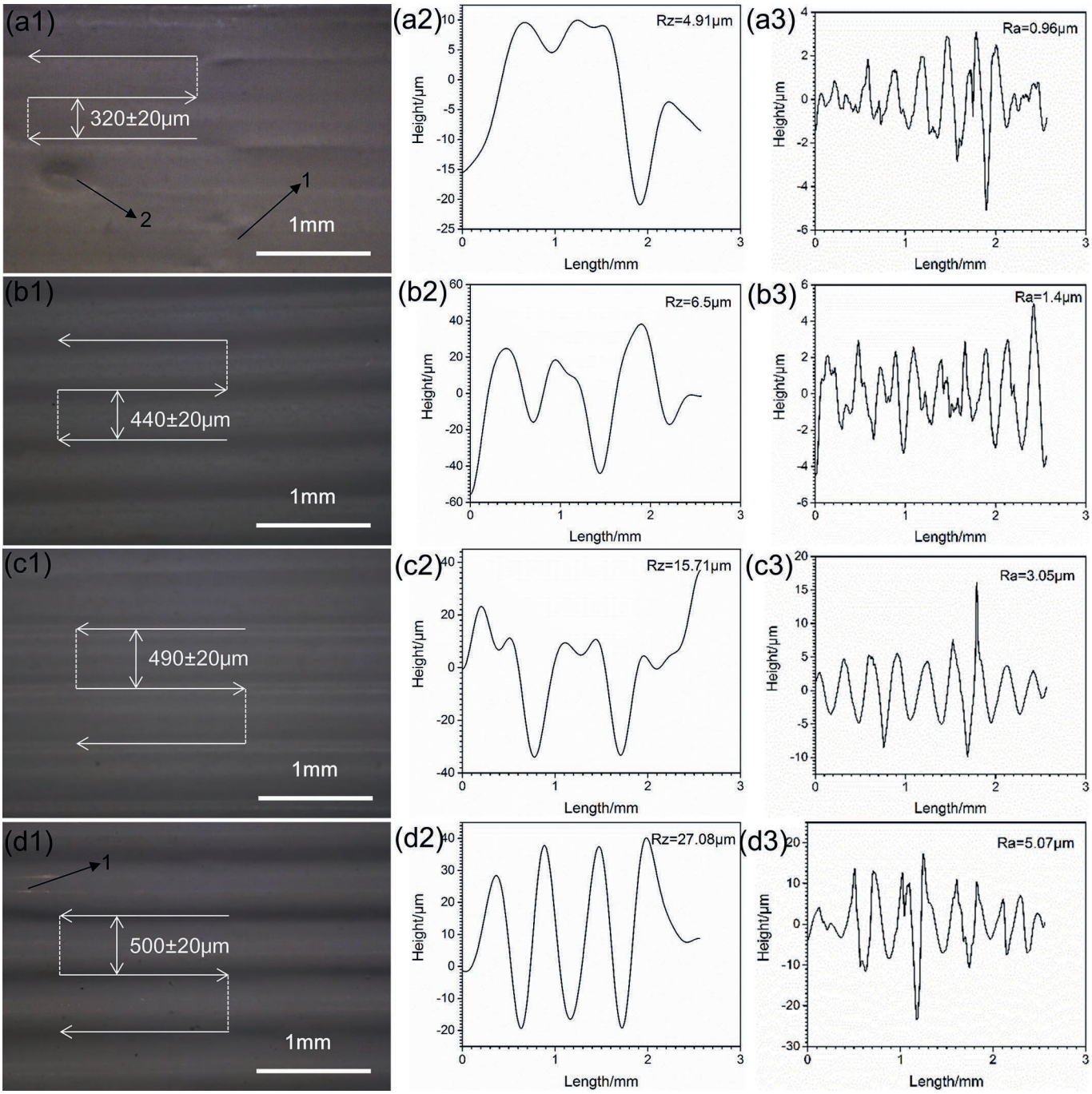


**Fig. 11:** Digital microscope top view, surface profile and roughness curve of sintered multi-layer sample at different overlap rates: (a) 11.1 %, (b) 6.4 %, (c) 1.6 %, (d) -4.1 %.

the "U"-shape between the layers is shown to be even, without obvious deformation, and the "U"-shape connection between the filaments is smooth. The "U"-shaped connection between the filaments in the same layer is almost a straight line, so that the boundary line is almost indistinct, indicating a robust bond. In Fig. 12(c), there is local concave deformation between the "U-shape" layers. As shown in Fig. 12(d), the "U"-shape connection between layers and filaments also exhibits an obvious boundary, which indicates that the overlap rate is too small. The mechanical extrusion and molecular diffusion between filaments cannot meet the gap between strands, the internal contact area of the sample is small, the bonding strength is low, and stratification is exhibited.

### *(3) Influence of internal structure on flexural strength*

Relative density is the actual density to the nominal counterpart. The nominal density of zirconia is 6.1 g/cm$^3$. The relative density and flexural strength of printed samples subject to different overlap rates are compared. When the overlap rate is 6.4 % and 11.1 %, respectively, the fracture surface density of the sample is uniform without obvious defects, indicating that there are no obvious gaps in the deposition process. After sintering, the relative density and bending strengths of the samples are relatively high, reaching 0.99, 0.99 and 676.23 MPa, 611.64 MPa respectively.

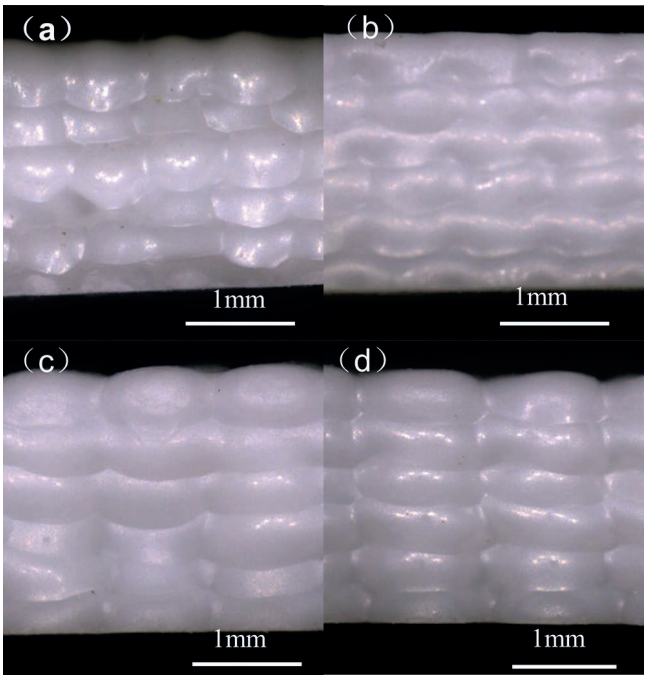


**Fig. 12:** Digital microscopic side view of printed samples with different overlap rates: (a) 11.1 %, (b) 6.4 %, (c) 1.6 %, (d) -4.1%.

When the overlapping rate is 1.6 % and -4.1 %, respectively, uneven pits are distributed on the fracture surface of the samples, indicating that during the deposition process, the adjacent slurry strands fail to completely fill the gap. After sintering, cracks tend to be incurred, leading to a significant decrease in the relative density and flexural strength of the samples, as shown in Fig. 13.

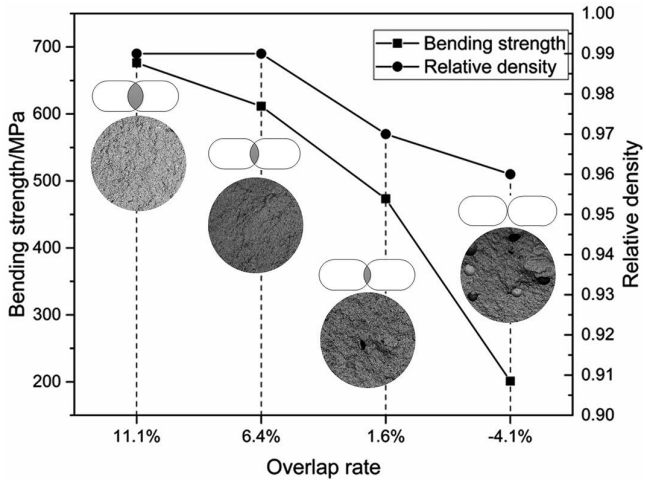


**Fig. 13:** Comparison of the mechanical properties of samples with different overlapping rates.

## VI. Conclusions

This paper explores the influence of the overlap rate on the forming quality for 3D-extrusion-based printing of zirconia ceramic slurry. With the currently proposed "collapse" and "overlap" models, ceramic samples with satisfactory surface morphology and mechanical properties are successfully printed. The following conclusions can be drawn.

For printing zirconia ceramic slurry with nozzles of different internal diameters (0.4 mm, 0.5 mm, 0.6 mm and 0.7 mm), the optimal ratio between the height of filament after collapse and the internal diameter of nozzle has been identified to be 0.96.

After the filaments are deposited and collapsed, for the nozzle with an internal diameter of 0.5 mm, the optimal overlap rate parameter is 6.4 %.

The overlap rate parameter is specified as 6.4 %, and the nozzle with an internal diameter of 0.5 mm is then adopted for 3D printing. After sintering, the waviness of the sample surface is 6.5 μm, the surface roughness is 1.4 μm, the relative density achieved is as high as 99 %, and the bending strength is as high as 611.64 MPa.

Setting of appropriate overlap rate can effectively reduce printing defects, and thus improve the printing quality. In this study, although the layer height of the filament can be predicted by the currently proposed models, the height between nozzle and the platform is yet to be explored. Our future research direction will therefore be to study the relationship between material characteristics and nozzle printing height. The ultimate target of our research is to establish a parameter system for the overall extrusion process and to extend its applicability to general extrusion printing for all other materials besides ceramic.

## V. Acknowledgments

This work was financially supported by the Key Research and Development Funding Project of Hebei Province (No. 17211808D) and Natural Science Foundation Funding Project of Tianjin (No. 18JCQNJC75100).

## References

1 State Administration for Market Regulation of the People's Republic of China, Standardization Administration of the People's Republic of China.GB/T 35021 – 2018 Additive manufacturing-Process categories and feedstock[S]. Beijing: Standards Press of China, 2018.

2 Aliheidari, N., Christ, J., Tripuraneni, R., Nadimpalli, S., Ameli, A.: Interlayer adhesion and fracture resistance of polymers printed through melt extrusion additive manufacturing process, *Mater. Design*., **156**, 351 – 361, (2018).

3 Santana, L., Ahrens, C.H., Netto, A.C.S., Bonin, C.: Evaluating the deposition quality of parts produced by an open-source 3D printer, *Rapid Prototyping J.*, **23**, 796 – 803, (2017).

4 Eiliat, H., Urbanic, J.: Visualizing, analyzing, and managing voids in the material extrusion process, *Int. J. Adv. Manuf. Tech.*, **96**, 4095 – 4109, (2018).

5 Comminal, R., Serdeczny, M.P., Pedersen, D.B., Spangenberg, J.: Motion planning and numerical simulation of material deposition at corners in extrusion additive manufacturing, *Addit. Manuf.*, **29**, 100753, (2019).

6 Chacón, J.M., Caminero, M.A., García-Plaza, E., Núñez, P.J.: Additive manufacturing of PLA structures using fused deposition modelling: effect of process parameters on mechanical properties and their optimal selection, *Mater. Design.*, **124**, 143 – 157, (2017).

7 Tang, S.Y., Yang, L., Li, G.J., Liu, X.W., Fan, Z.T.: 3D printing of highly-loaded slurries via layered extrusion forming: parameters optimization and control, *Addit. Manuf.*, **28**, 546 – 553, (2019).

8 Plessis, A.: Effects of process parameters on porosity in laser powder bed fusion revealed by X-ray tomography, *Addit. Manuf.*, **30**, 100871, (2019).

[9] Gu, H., Lian, Q., Wang, H.C., Li, D.C., Jin, G.R., Cui, B.: Extrusion 3D printing processes and performance evaluation of GelMA composite hydrogel, *Chin. J. Mech. Eng-En.*, **56**, 196 – 204, (2020).

[10] Liu, C., Xu, M.E., Wang, L., Song, J.X.: Simulation and construction of vascular channel in 3D printed cell culture scaffold, *CHINA Biotechn.*, **36**,67 – 74, (2017).

[11] Godoi, F.C., Prakash, S., Bhandari, B.R.: 3d printing technologies applied for food design: status and prospects, *J. Food. Process. Eng.*, **179**, 44 – 54, (2016).

[12] Smay, J.E., Cesarano, J., Lewis, J.A.: Colloidal inks for directed assembly of 3-D periodic structures, *Langmuir*, **18**, 5429 – 5437, (2002).

[13] Perrot, A., Rangeard, D., Pierre, A.: Structural built-up of cement-based materials used for 3D-printing extrusion techniques, *Mater. Struct.*, **49**, 1213 – 1220, (2016).

[14] Le, T.T., Austin, S.A., Lim, S., Buswell, R.A., Gibb, A.G.F., Thorpe, T.: Mix design and fresh properties for high-performance printing concrete, *Mater. Struct.*, **45**, 1221 – 1232, (2012).

[15] Zhu, S.C., Stieger, M.A., Goot, A.J., Schutyser, M.A.I.: Extrusion-based 3D printing of food pastes: correlating rheological properties with printing behaviour, *Innov. Food Sci. Emerg.*, **58**, 102214, (2019).

[16] Costakis, W.J., Rueschhoff, L.M., Diaz-Cano, A.I., Youngblood, J.P., Trice, R.W.: Additive manufacturing of boron carbide via continuous filament direct ink writing of aqueous ceramic suspensions, *J. Eur. Ceram. Soc.*, **14**, 3249 – 3256, (2016).

[17] Rueschhoff, L., Costakis, W., Michie, M., Youngblood, J., Trice, R.: Additive manufacturing of dense ceramic parts via direct ink writing of aqueous alumina suspensions, *Int. J. Appl. Ceram. Tec.*, **13**, 821 – 830, (2016).

[18] Shaw, L., Islam, M., Li, J., Li, L., Imran Ayub, S.M.: High-speed additive manufacturing through high-aspect-rate nozzles, *JOM-US.*, **70**, 284 – 291, (2018).

[19] Turner, B.N., Gold, S.A.: A review of melt extrusion additive manufacturing processes: II. materials, dimensional accuracy, and surface roughness, *Rapid Prototyping J.*, **21**, 250 – 261, (2015).

[20] Sun, Q., Rizvi, G.M., Bellehumeur, C.T., Gu, P.: Effect of processing conditions on the bonding quality of FDM polymer filaments, *Rapid Prototyping J.*, **14**, 72 – 80, (2008).

[21] Ji, Z.H., Zhao, D.C., Hao, J.J., Zhang, X.D., Wang, J.Z.: 3D gel-printing of TiC-reinforced 316L stainless Steel: influence of the printing parameters, *J. Mater. Eng. Perform.*, **27**, 5500 – 5510, (2018).

[22] Comminal, R., Serdeczny, M.P., Pedersen, D.B., Spangenberg, J.: Numerical modeling of the strand deposition flow in extrusion-based additive manufacturing, *Addit. Manuf.*, **20**, 68 – 76, (2018).

[23] Luo, B., Xia, H.F., Chen, H.L., Zhu, Z.C., He, X.M., Li, D.C.: Three-dimensional printing technology of ionic gel materials, *Chin. J. Mech. Eng-en.*, **54**, 157 – 164, (2008).

[24] Serdeczny, M.P., Comminal, R., Pedersen, D.B., Spangenberg, J.: Numerical simulations of the mesostructure formation in material extrusion additive manufacturing, *Addit. Manuf.*, **28**, 419 – 429, (2019).

[25] Eiliat, H., Urbanic, J.: Determining the relationships between the build orientation, process parameters and voids in additive manufacturing material extrusion processes, *Int. J. Adv. Manuf. Tech.*, **100**, 683 – 705, (2019).

[26] Wang, J., Chen, T.W., Jin, Y.A., He, Y.: Variable bead width of material extrusion-based additive manufacture, *J. Zhejiang. Univ-Sc. A.*, **20**, 73 – 82, (2019).